Integration of diploid T2T parental genomes with progeny genomes and transcriptomes identifies resistance genes in the grape powdery mildew resistance loci *Ren6* and *Ren7* of *Vitis piazeskii*

Mélanie Massonnet[1], Rosa Figueroa-Balderas[1], Noé Cochetel[1], Summaira Riaz[1], Dániel Pap[1], M. Andrew Walker[1], Dario Cantu[1,2*]

[1]Department of Viticulture and Enology, University of California Davis, Davis, CA, 956161, USA
[2] USDA-ARS,
[3]Genome Center, University of California Davis, Davis, CA, 95616, USA

[*]Corresponding author:
dacantu@ucdavis.edu

Abstract

The Chinese grape accession *Vitis piasezkii* DVIT2027 carries two loci associated with powdery mildew (PM) resistance, *Ren6* and *Ren7*. Although these loci differ in the timing and strength of their response to *Erysiphe necator*, both are consistent with recognition by intracellular immune receptors. Here, we aimed to identify the nucleotide-binding leucine-rich repeat (NLR) genes responsible for PM resistance within *Ren6* and *Ren7*. To do so, we assembled diploid telomere-to-telomere (T2T) genomes of *V. piasezkii* DVIT2027 and *V. vinifera* F2-35, the resistant and susceptible parents, respectively, of a segregating F1 population. We then integrated these assemblies with deep resequencing data from eight F1 sib-lines carrying different combinations of *Ren6* and *Ren7*, and generated trio-binned, parent-phased genomes for six of them. This allowed us to resolve and phase the *Ren6* and *Ren7* loci and their PM-susceptible alternative haplotypes. Comparative analyses revealed extensive structural variation, particularly duplications, and numerous short polymorphisms between resistant and susceptible haplotypes, leading to complete sequence specificity among all NLRs in *Ren6* and *Ren7*, with several lacking allelic counterparts in their respective susceptible haplotypes. Expression profiling across PM-resistant sib-lines identified four and two candidate CC-NBS-LRR genes associated with *Ren6* and *Ren7*, respectively, based on both expression and haplotype specificity. These results provide a high-resolution view of two key PM resistance loci and support the identification of candidate resistance genes for functional validation and targeted grapevine breeding.

Keywords: powdery mildew resistance, *Vitis piasezkii*, NLR genes, telomere-to-telomere diploid genome assembly, *Ren6*, *Ren7*, haplotype phasing, grapevine breeding

Introduction

Cultivated grapevines belonging to *V. vinifera* spp. *vinifera* (hereafter *V. vinifera*) are mostly susceptible to powdery mildew (PM). In grapes, PM is caused by the obligate biotrophic ascomycete *Erysiphe necator* Schwein. (syn. *Uncinula necator*). *E. necator* can infect any green tissue of a grapevine, including leaves, canes, inflorescences, and green berries (Gadoury et al., 2011). PM reduces leaf photosynthetic capacity and negatively impacts fruit yield, fruit composition, and wine quality (Calonnec et al., 2004; Stummer et al., 2005). To control the disease, fungicides are routinely applied as a preventive measure; however they are costly (Sambucci et al., 2019). Another approach to control PM is the use of resistant grapevine cultivars developed through the introgression of genetic loci associated with PM resistance. Fifteen PM resistance-associated loci have been genetically mapped in wild *Vitis* species and in *Muscadinia rotundifolia*, and are referred to as *Resistance to Uncinula necator* (*Run*) or *Resistance to Erysiphe necator* (*Ren*) (Dry et al., 2019; Karn et al., 2021; Ricciardi et al., 2024). Although the introgression of PM resistance loci into grapevine cultivars has conferred complete or partial resistance to the disease, it has also resulted in substantial linkage drag from the wild genetic background (Foria et al., 2022). Elimination of unwanted wild genetic material has been hampered by the inherently low recombination rates in grape breeding programs, and by the lack of perfect markers, i.e., markers specific to the resistance (*R*) genes, which is is primarily due to the limited knowledge of the genes responsible for disease resistance. So far, only one *R* gene, encoding an intracellular receptor, has been characterized as contributing to PM resistance in grapes (Feechan et al., 2013). This gene was identified twelve years ago at the *Run1* locus from *M. rotundifolia* G52 using bacterial artificial chromosome (BAC) walking. Recent developments in grape genomics, including the availability of diploid genome assemblies (Cantu et al., 2024), have enabled the identification of candidate *R* genes at several PM resistance loci (Paineau et al., 2024). In this study, we leveraged recent genomic advances to identify candidate *R* genes in the PM resistance loci *Ren6* and *Ren7* of *V. piasezkii* DVIT2027.

Ren6 and *Ren7* loci were identified through quantitative trait locus (QTL) mapping of the F1 population 11373, derived from a cross between the PM-susceptible (PMS) *V. vinifera* F2-35 and the PM-resistant (PMR) *V. piasezkii* DVIT2027 (Pap et al., 2016). *Ren6* and *Ren7* were mapped to chromosome 9 and 19, respectively; both in heterozygous state. Although both loci confer PM resistance, the speed and strength of their responses to the pathogen differ significantly. *Ren6* confers complete resistance while *Ren7* leads to a reduction in colony size. In both cases, PM resistance involves the induction of programmed cell death (PCD) in epidermal cells penetrated by *E. necator* appressoria; appressoria of germinated spores for *Ren6*, and appressoria of developing secondary hyphae for *Ren7*. Because PCD occurs post-penetration of the pathogen, it likely results from the recognition of effectors secreted by *E. necator* by specific intracellular receptors belonging to *Ren6* and *Ren7* loci (Pap et al., 2016).

Nucleotide-binding domain and leucine-rich repeat (NLR) proteins are intracellular receptors that activate plant immune responses upon pathogen recognition (Chia and Carella, 2023). Canonical NLRs are composed of three domains: a variable N-terminal domain, a central nucleotide-binding site domain (NBS), and a C-terminal leucine-rich repeat (LRR) domain. Most plant NLRs possess N-terminal domains classified as coiled-coil (CC), Resistance to Powdery Mildew 8 (RPW8), or Toll/interleukin-1 receptor (TIR) types (Lolle et al., 2020). The C-terminal LRR region of the NLRs mediates effector recognition, either directly or indirectly, while the N-terminal domain

participates in the formation of large oligomeric complexes, known as resistosomes, that initiate NLR immune signaling (Chia and Carella, 2023; Locci and Parker). NLR-triggered immune responses include Ca^{2+} influx, reactive oxygen species bursts, and an extensive transcriptional reprogramming (Lolle et al., 2020). In addition, NLR activation often induces a hypersensitive response, a rapid and localized form of PCD at the infection site (Lolle et al., 2020).

In this study, we aimed to identify NLR genes potentially responsible for PM resistance within the two *R* loci of *V. piasezkii* DVIT2027, *Ren6* and *Ren7*. We first generated diploid telomere-to-telomere (T2T) genome assemblies of *V. piasezkii* DVIT2027 and the maternal parent of the 11373 population, *V. vinifera* F2-35. We then verified the structure, sequence and phasing of *Ren6*, *Ren7*, and their PMS alternative haplotypes using deep sequencing data from eight 11373 sib-lines with different *R* locus composition, along with the parent-phased genomes of six of them. NLR genes located within the two *R* loci and their corresponding PMS haplotypes were identified and manually curated. To pinpoint the NLR genes specific to *Ren6* and *Ren7*, we compared each *R* locus with its respective PMS haplotype to identify structural variations affecting NLR gene content or domain composition. We also assessed the allelic relationships between NLRs at the *Ren6* and *Ren7* loci and those at the PMS haplotypes. Finally, to prioritize NLR genes potentially associated with PM resistance, we profiled their expression in six PMR 11373 sib-lines carrying different combinations of *Ren6* and *Ren7* using RNA sequencing (RNA-seq).

Materials and Methods

Plant material and PM inoculation

Young leaves from *V. piazeskii* DVIT2027, *V. vinifera* F2-35, and eight of their progeny (Pap et al., 2016): 11373-158 (*Ren6*$^+$/*Ren7*$^-$), 11373-195 (*Ren6*$^+$/*Ren7*$^-$), 11373-137 (*Ren6*$^-$/*Ren7*$^+$), 11373-257 (*Ren6*$^-$/*Ren7*$^+$), 11373-098 (*Ren6*$^+$/*Ren7*$^+$), 11373-145 (*Ren6*$^+$/*Ren7*$^+$), 11373-130 (*Ren6*$^-$/*Ren7*$^-$), and 11373-156 (*Ren6*$^-$/*Ren7*$^-$), were collected for genome sequencing.
For gene expression profiling, PM was inoculated as described in Amrine *et al*. (Amrine et al., 2015). Three plants of each grape accession were inoculated with *E. necator* C-train, meanwhile three other plants were mock-inoculated. At 1 and 5 dpi, two leaves from each plant were pooled together to constitute a biological replicate, and immediately frozen in liquid nitrogen. Therefore, each condition was represented by three biological replicates.

DNA and RNA extraction, library preparation, and sequencing

High-molecular weight genomic DNA was isolated from young leaves of *V. piazeskii* DVIT2027, *V. vinifera* F2-35, 11373-158 (*Ren6*$^+$/*Ren7*$^-$), 11373-137 (*Ren6*$^-$/*Ren7*$^+$), 11373-098 (*Ren6*$^+$/*Ren7*$^+$), 11373-145 (*Ren6*$^+$/*Ren7*$^+$), 11373-130 (*Ren6*$^-$/*Ren7*$^-$), and 11373-156 (*Ren6*$^-$/*Ren7*$^-$) as in Chin *et al*. (Chin et al., 2016). DNA quantity was assessed using a Qubit™ 1X dsDNA HS Assay Kit (Thermo Fisher, MA, USA), DNA purity with a Nanodrop 2000 spectrophotometer (Thermo Scientific, IL, USA), DNA integrity using the DNA High Sensitivity kit (Life Technologies, CA, USA) and by pulsed-field gel electrophoresis. HiFi libraries of *V. piazeskii* DVIT2027 and *V. vinifera* F2-35 were prepared as Minio *et al*. (Minio et al., 2022a) and sequenced with a PacBio Revio platform. SMRTbell libraries of the progeny was made like Minio *et al*. (Minio et al., 2019a) and sequenced using PacBio Sequel II system (Pacific Biosciences, CA, USA) (**Table S1**).
DNA extraction and short-read DNA sequencing (DNA-seq) library preparation were performed as Massonnet *et al*. (Massonnet et al., 2020). DNA libraries were sequenced as 150-bp paired-end

128 reads using an Illumina HiSeq3000 for *V. vinifera* F2-35 library, and an HiSeqX Ten system for
129 the others (IDseq, Davis, CA, USA).
130 Total RNA was extracted with a cetyltrimethylammonium bromide (CTAB)-based protocol as
131 described in Cochetel *et al*. (Cochetel et al., 2021). RNA quantity was evaluated with a Qubit 2.0
132 Fluorometer and a broad-range RNA kit (Life Technologies, CA, USA), RNA purity with a
133 Nanodrop 2000 spectrophotometer (Thermo Scientific, IL, USA), RNA integrity through
134 electrophoresis and with an Agilent 2100 Bioanalyzer (Agilent Technologies, CA, USA). cDNA
135 library preparation was made as in Amrine *et al*. (Amrine et al., 2015). cDNA library of young
136 leaves of *V. piasezkii* DVIT2027 was sequenced as 100-bp single-end reads by an Illumina
137 HiSeq3000. Concerning the PM- and mock-inoculated leaves of the 11373 sib-lines, cDNA
138 libraries were sequenced using an Illumina HiSeq2500 sequencer (DNA Technologies Core,
139 University of California, Davis, CA, USA) as 50-bp single-end reads (**Table S2**). Full-length
140 cDNA sequencing library was prepared from young leaves of *V. piazeskii* DVIT2027 and
141 sequenced as in Cochetel *et al*. (Cochetel et al., 2023).
142
143 **Genome assembly**
144 For *V. piazeskii* DVIT2027 and *V. vinifera* F2-35, PacBio HiFi reads were first subsampled to 60X
145 coverage using with seqtk sample from the package seqtk v.1.2-r101-dirty
146 (https://github.com/lh3/seqtk) and the parameter "-s100", and then assembled using hifiasm
147 (Cheng et al., 2021) with the option "-n 13" (**Table S3**). Contigs were scaffolded into chromosome-
148 scale pseudomolecules for both haplotypes using HaploSync v1.0 (Minio et al., 2022b) and a
149 consensus grape synteny map. Telomere repeat units were searched using TIDK v.0.2.63
150 (https://github.com/tolkit/telomeric-identifier); tidk explore with the options "--minimum 5 --
151 maximum 12 -t 2 --log"; tidk search with the option "-s TTTAGGG". Results were visualized with
152 tidk plot. BUSCO v.5.4.7 with the library embryophyte_odb10 (Waterhouse et al., 2018) were
153 used to evaluate the gene space completeness of the genome assemblies. Concerning the six F1
154 individuals (11373-158, 11373-137, 11373-098, 11373-145, 11373-130, 11373-156), genome
155 assembly of the PacBio CLR reads was performed using Canu v2.2 and short DNA-seq reads from
156 the two parents (Koren et al., 2018). For sequence polishing, PacBio CLR reads were first aligned
157 on the genome assembly using the bioconda package pbmm2 v.1.9.0
158 (https://github.com/PacificBiosciences/pbmm2). Polishing was then performed with the bioconda
159 package pbgcpp v.2.0.2-2.0.2 (https://github.com/PacificBiosciences/gcpp; downloaded August
160 11th, 2022) using the Arrow algorithm (**Table S2**).
161
162 **Genome annotation**
163 Repetitive elements were annotated using RepeatMasker v.4.1.7-p1
164 (http://www.repeatmasker.org) and a grape repeat library (Minio et al., 2019b). A set of high-
165 quality gene models was created using PASApipeline v2.5.3
166 (https://github.com/PASApipeline/PASApipeline), GMAP v.2024-11-20 (Wu and Watanabe,
167 2005), and pblat v.2.5.1 (Wang and Kong, 2019). As transcriptomic evidence, we used the
168 PN40024.v5.1 predicted protein-coding sequences (https://grapedia.org/t2t_annotation/), and the
169 high-quality isoforms of *V. piazeskii* DVIT2027, and Cabernet Sauvignon (Minio et al., 2019b)
170 for *V. vinifera* F2-35. Transcripts were extracted from the Iso-Seq reads of *V. piazeskii* DVIT2027
171 young leaves like Cochetel *et al*. (Cochetel et al., 2023). The set of high-quality gene models was
172 used as input for the *ab initio* predictors Augustus v.3.5.0 (Stanke et al., 2006) and GeneMark v.
173 3.68_lic (Lomsadze et al., 2005). EvidenceModeler v.2.1.0 (Haas et al., 2008) was then used to

174 generate consensus models from the gene models produced by the *ab initio* predictions and PASA.
175 Gene models encoding protein sequences with a length inferior to 50 amino acids, in-frame stop
176 codons, no start methionine, no stop codon, were removed.
177
178 **Functional annotation**
179 Predicted proteins of *V. piazeskii* DVIT2027 and *V. vinifera* F2-35 genomes were aligned onto the
180 proteins of *Arabidopsis thaliana* (Araport11_genes.201606.pep.fasta;
181 https://www.arabidopsis.org/download/index.jsp) using BLASTP v.2.12.0+ (Altschul et al.,
182 1990). Alignments with an identity greater than 30%, and both reference:query and
183 query:reference coverages between 75% and 125%, were retained. Among the remaining
184 alignments, the alignment with the highest product of identity, query coverage, and reference
185 coverage, was selected for each grape protein to determine its homolog in *A. thaliana*. Same
186 methods were used to identify homologous proteins in the grape *V. vinifera* PN40024 genome
187 (Jaillon et al., 2007)(V1 annotation).
188 Protein domains were searched using hmmsearch from HMMER v.3.3.1 (http://hmmer.org/) and
189 the Pfam-A Hidden Markov Models (HMM) database (El-Gebali et al., 2019)(downloaded on
190 March 12th, 2025). Protein domains with an independent E-value <1.0, and at least 50% of the
191 HMM were selected. Coiled coils (CC) domains were identified using COILS (Lupas et al., 1991).
192 Functional annotation of the predicted proteins of *V. piazeskii* DVIT2027 and *V. vinifera* F2-35
193 genomes can be retrieved in **Tables S4-S5**.
194
195 **NLR gene annotation**
196 Gene loci potentially encoding NLRs were detected among *V. piazeskii* DVIT2027 and *V. vinifera*
197 F2-35 genomes with NLR-Annotator using default parameters (Steuernagel et al., 2020). To assess
198 the intron-exon structure of the potential NLR genes within the *R* loci and the PMS alternative
199 haplotypes, RNA-seq reads from *V. piazeskii* DVIT2027, *V. vinifera* F2-35, and their eight
200 progeny lines were aligned on the combined genomes of *V. piazeskii* DVIT2027, *V. vinifera* F2-
201 35, and *E. necator* C-strain (Jones et al., 2014), using HISAT2 v.2.1.0 (Kim et al., 2015) and the
202 parameters "--end-to-end --sensitive -k 50". RNA-seq reads of *V. vinifera* F2-35 were retrieved
203 from the NCBI BioProject PRJNA897013 (Massonnet et al., 2022a). Alignments were visualized
204 in Integrative Genomics Viewer v.2.4.14 (Robinson et al., 2011). Manual refinement of the NLR
205 gene models was performed when the alignments of RNA-seq reads indicated a different intron-
206 exon structure than the *ab initio* structural annotation.
207 LRR motifs among the candidate NLRs were predicted using LRRpredictor v1.0 (Martin et al.,
208 2020).
209
210 ***Ren6* and *Ren7* region localization**
211 The loci *Ren6* and *Ren7* and their alternative haplotypes were located by *in silico* amplification of
212 the *Ren6*- and *Ren7*-associated markers (**Table S6**) described in Pap *et al*. (Pap et al., 2016) on the
213 genome assemblies using dipr (https://github.com/douglasgscofield/dispr).
214
215 **Haplotype coverage analysis**
216 To confirm the phasing of the *Ren6* and *Ren7* haplotypes and their alternative haplotypes in the
217 genomes of *V. piazeskii* DVIT2027 and *V. vinifera* F2-35, we used the short DNA-seq reads from
218 the eight F1 lines, *V. piazeskii* DVIT2027 and *V. vinifera* F2-35. Adapter sequences and low-
219 quality reads were removed using Trimmomatic v.0.36 (Bolger et al., 2014) with the following

parameters: "LEADING:3 TRAILING:3 SLIDINGWINDOW:10:20 MINLEN:36 CROP:150". High-quality reads were then aligned onto the combined genomes of *V. piazeskii* DVIT2027 and *V. vinifera* F2-35 using BWA v0.7.17 (Li and Durbin, 2009) with default parameters. Reads aligning perfectly to the reference genome were selected with bamtools filter v.2.5.1 (Barnett et al., 2011) and the option "NM:0". Base coverage was performed using genomecov from BEDTools v2.29.1 (Quinlan, 2014). Coverage in repetitive elements was removed using BEDTools intersect. Median coverage per window of 10-kbp was computed by BEDTools map. For each grape accession, the median coverage per 10-kbp window was normalized by dividing by the sequencing coverage of the accession (**Table S2**).

Sequence comparison

Pairwise sequence alignments of whole haplotypes were done with NUCmer from MUMmer v.4.0.0 (Marçais et al., 2018) with the "--mum" option. For the alignment of 11373 sib-lines' genomes onto *Ren6*, *Ren7*, and their alternative haplotypes, each parental genome was aligned onto the parent haplotypes. Alignments longer than 5 kbp were retained using the parameters "-l 5000". Regarding the comparison between PMR and PMS haplotypes, alignments with at least 90% identity are represented in **Figure 2**. Structural variants (SVs; >50 bp) were called using show-diff from MUMmer v.4.0.0 with defaults parameters. SNPs and INDELs (<50 bp) were detected using show-snps from MUMmer v.4.0.0.

To assess whether NLR genes of *Ren6* and *Ren7* loci were present in *V. piazeskii* 0957 and BL-1, CDS of the NLR genes composing the two *R* loci were first aligned onto the four haploid genomes using GMAP v.2020-06-01 (Wu and Watanabe, 2005) (**Tables S7-S8**). Resulting alignments were then used to generate proteins by gffread from Cufflinks v.2.2.1 (Trapnell et al., 2010).

Protein alignments were performed using BLAST v.2.2.28+ (Altschul et al., 1990).

Gene expression analysis

High-quality reads were obtained using Trimmomatic v.0.36 (Bolger et al., 2014) with the following parameters: "LEADING:3 TRAILING:3 SLIDINGWINDOW:10:20 MINLEN:36" (**Table S9**). Transcript abundance was evaluated with Salmon v.1.5.1 (Patro et al. 2017). First, the transcriptome index file was built using the combined protein-coding sequences of *V. piazeskii* DVIT2027 and *V. vinifera* F2-35, and *E. necator* C-strain (Jones et al., 2014), their genomes as decoys, and the options: "-k 13 --keepDuplicates". Second, transcript abundance was quantified with the parameters "--gcBias –seqBias --validateMappings". Read counts from *E. necator* C-strain were removed, and gene expression in transcript per million (TPM) from the grape CDS were calculated.

Results

Haplotype-resolved T2T genome assemblies of *V. piazeskii* DVIT2027 and *V. vinifera* F2-35

To identify *R* genes potentially involved in PM resistance of *V. piazeskii* DVIT2027, we sequenced the genomes of the paternal (*V. piazeskii* DVIT2027) and maternal (*V. vinifera* F2-35) parents of the 11373 population (Pap et al., 2016), using long-read DNA sequencing (PacBio HiFi reads; **Table S1**). Draft haplotype-resolved genome assemblies of *V. piazeskii* DVIT2027 and *V. vinifera* F2-35 were composed of 120 and 238 contigs, respectively, resulting in a total size of 1,018.8 and 975.7 Mbp, respectively (**Table S3**). Pseudomolecule reconstruction resulted in two sets of nineteen chromosomes of 504.6 Mbp (Hap1) and 507.1 Mbp (Hap2) for *V. piazeskii* DVIT2027,

266 and 481.3 Mbp (Hap1) and 481.5 Mbp (Hap2) for *V. vinifera* F2-35 (**Table 1**). The difference of
267 length between the two genome assemblies (38.1 Mbp) was mostly due to larger chromosomes
268 12,13, 16, 17, and 18 in *V. piazeskii* DVIT2027 compared to *V. vinifera* F2-35 (**Table S10**). This
269 size difference was made of repetitive elements (49.2%), but also of protein-coding gene loci
270 (12.3%).
271
272 Contigs not anchored to pseudomolecules accounted for only 0.7 and 1.9 % of the genome size for
273 *V. piazeskii* DVIT2027 and *V. vinifera* F2-35, respectively, and were predominantly composed of
274 repetitive elements (**Table 1**). The haplotypes of the two genomes contained 99.3 ± 0.2 % of the
275 Benchmarking Universal Single-Copy Orthologs (BUSCOs), indicating high completeness. On
276 average, 32.8 ± 1.3 telomeres of the 38 possible telomeres were observed in the pseudomolecules
277 of each haplotype. Together, these results demonstrate that we generated highly contiguous,
278 haplotype-resolved genomes for both parents of the 11373 population.
279
280 **Table 1**: Statistics of the genome assemblies of *V. piazeskii* DVIT2027 and *V. vinifera* F2-35.

	***V. piasezkii* DVIT2027**			***V. vinifera* F2-35**		
	Hap 1	**Hap 2**	**Unplaced**	**Hap 1**	**Hap 2**	**Unplaced**
Assembly length (Mbp)	504.6	507.1	7.6	481.3	481.5	18.4
Number of sequences	19	19	55	19	19	93
Average length (Mbp)	26.6	26.7	0.1	25.3	25.3	0.2
Telomeres	31/38	33/38	0	34/38	33/38	0
Number of gene loci	34,926	31,353	652	29,820	29,399	394
Gene content (Mbp)	149.6	134.3	1.7	141.9	138.1	0.9
Repeats (Mbp)	284.1	285.0	5.5	270.0	270.0	15.8
Repeats (%)	56.3	56.3	71.9	56.1	56.1	85.9
BUSCO (%)	99.3	99.5	0.6	99.4	99.1	0.2

281
282 **Identification and haplotype phasing of *Ren6* and *Ren7* loci of *V. piazeskii* DVIT2027**
283 The boundaries of the *Ren6* and *Ren7* haplotypes and their PMS alternative haplotypes were
284 defined by *in silico* amplification of the *Ren6*-associated markers PN9-057 and VMC4h4.1, and
285 *Ren7*-associated markers VMC9a2.1 and VVIu09 (Pap et al., 2016) on the diploid genomes of *V.*
286 *piazeskii* DVIT2027 and *V, vinifera* F2-35. In the *V. piazeskii* DVIT2027 genome, the *Ren6* and
287 *Ren7* loci measured 927.5 and 791.6 kbp, respectively, whereas their PMS alternative haplotypes
288 were 1,380.1 and 771.1 kbp, respectively (**Table 2**). In *V. vinifera* F2-35, all PMS alternative
289 haplotypes to *Ren6* and *Ren7* loci were shorter than those of *V. piazeskii* DVIT2027, measuring
290 771.1 and 870.7 kbp for *Ren6* alternatives, and 537.4 and 570.3 kbp for *Ren7* alternatives (**Figure**
291 **1**).
292
293 **Table 2**: Characteristics of the *Ren6* and *Ren7* loci and their alternative PM-susceptible (PMS)
294 haplotypes in *V. piazeskii* DVIT2027 and *V. vinifera* F2-35.
295

Grape accession	***V. piasezkii* DVIT2027**	***V. vinifera* F2-35**

Locus	*Ren6*	*Ren6*-PMS alternative	*Ren7*	*Ren7*-PMS alternative	*Ren6*-PMS alternative Hap1	*Ren6*-PMS alternative Hap2	*Ren7*-PMS alternative Hap1	*Ren7*-PMS alternative Hap2
Chromosome	Chr09 Hap1	Chr09 Hap2	Chr19 Hap1	Chr19 Hap2	Chr09 Hap1	Chr09 Hap2	Chr19 Hap1	Chr19 Hap2
Start-Stop (bp)	8,626,384-9,553,923	9,061,939-10,442,008	883,779-1,675,391	951,279-1,750,630	8,690,011-9,461,149	8,080,301-8,951,049	904,827-1,442,232	843,589-1,413,925
Length (bp)	927,540	1,380,070	791,613	799,352	771,139	870,749	537,406	570,337
Protein-coding gene loci	54	80	81	77	42	50	49	56
Total NLR genes	19	35	13	8	12	12	2	3
CC-NBS-LRR	15	25	10	6	10	8	2	2
CC-NBS	2	5	0	1	1	2	0	0
NBS-LRR	2	4	3	1	1	2	0	1
NBS	0	1	0	0	0	0	0	0

To examine the structure, sequence, and haplotype phasing of the *Ren6* and *Ren7* loci and their PMS counterparts, we applied two approaches: (i) assessing the normalized median base coverage per 10 kbp of *V. piazeskii* DVIT2027 and *V. vinifera* F2-35 haplotypes using deep sequencing data of eight sib-lines from population 11373 (Pap et al., 2016); and (ii) aligning the parent-phased genomes of six out of the eight sib-lines onto the *V. piazeskii* DVIT2027 and *V. vinifera* F2-35 haplotypes. For the base coverage analysis, the eight F1 lines included: two lines (11373-158 and 11373-195) carrying *Ren6* (*Ren6*$^{+}$) and the alternative PMS haplotype of *Ren7* (*Ren7*$^{-}$); two lines only having *Ren7* (*Ren6*$^{-}$/*Ren7*$^{+}$; 11373-137 and 11373-137); two lines with both *Ren6* and *Ren7* loci (*Ren6*$^{+}$/*Ren7*$^{+}$; 11373-098 and 11373-145); two lines devoid of both *Ren6* and *Ren7* loci (*Ren6*$^{-}$/*Ren7*$^{-}$; 11373-130 and 11373-156). Short-read DNA-seq data from *Ren6*$^{+}$ and *Ren7*$^{+}$ accessions showed 1x coverage at the respective loci (**Figure S1-S2**), with similar results observed for their PMS alternative haplotypes (**Figure S3-S4**). These results indicate that no haplotype switching occurred during the assembly of *V. piazeskii* DVIT2027. In *V. vinifera* F2-35, the normalized base coverage profiles confirmed the inheritance of PMS haplotypes in the F1 sib-lines, with no evidence of recombination or haplotype switching (**Figure S5-S8**).

To further validate the structure, sequence, and phasing of *Ren6* and *Ren7* loci and their PMS counterparts, we generated genomes of six of the eight sib-lines using PacBio CLR reads and a trio-binning genome assembly approach (Koren et al., 2018)(**Table S3**). Each sib-line genome consisted of two haploid parent-phased assemblies: one attributed to *V. piazeskii* DVIT2027 and the other to *V. vinifera* F2-35. Alignment of the six assemblies onto *Ren6*, *Ren7*, and their PMS haplotypes showed complete coverage by the sib-line contigs (**Figure 1**). The *Ren6*- and *Ren7*-PMS haplotypes of *V. piazeskii* DVIT2027 were the only haplotypes not covered by a single contig in one sib-line. Alignments had an average identity of 99.96 ± 0.04 % (**Figure 1**). Together, these results validate the structure, sequence, and phasing of the haplotypes in both parents, *V. piazeskii* DVIT2027 and *V. vinifera* F2-35.

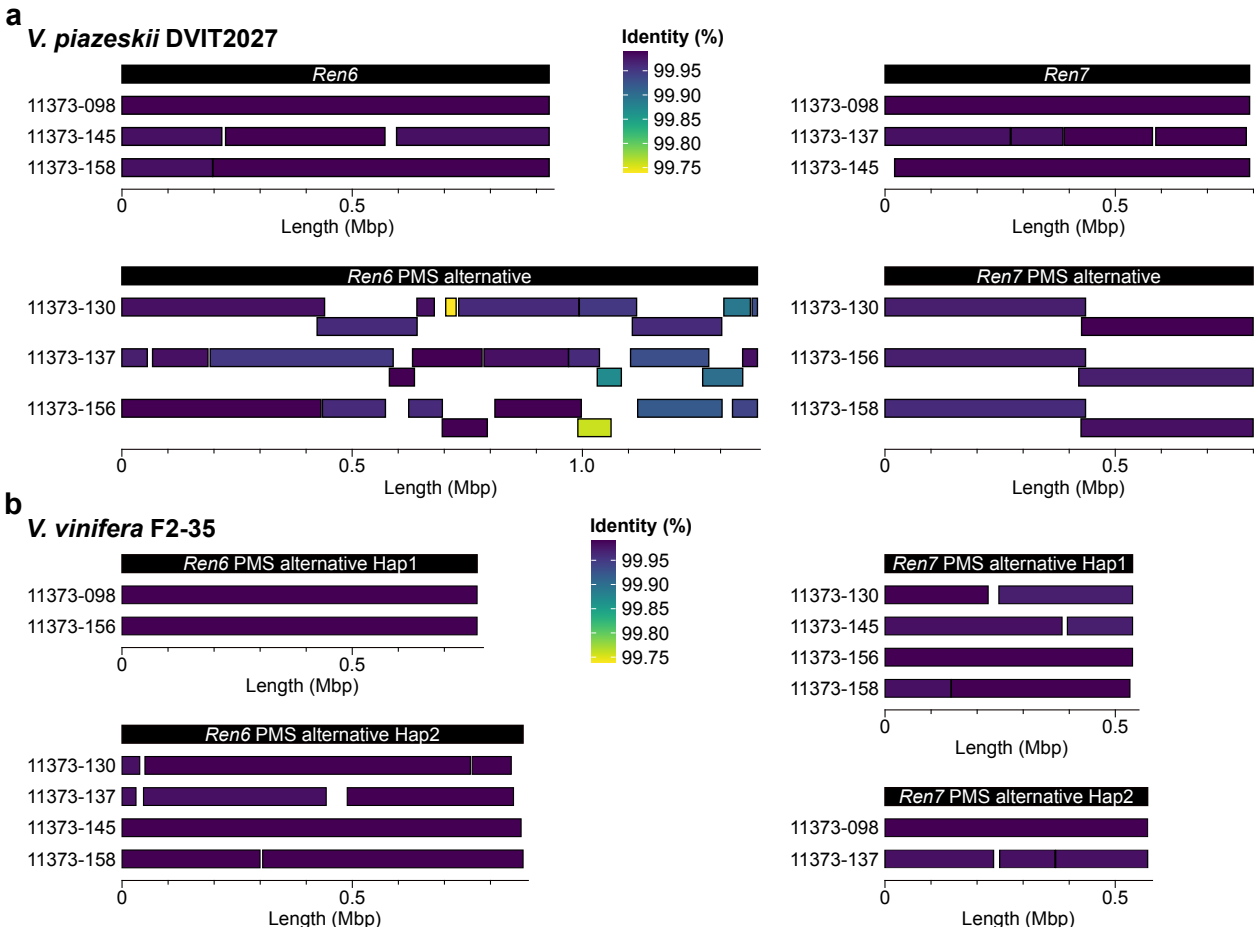

Figure 1: Verification of the structure, sequence, and haplotype phasing of *Ren6* and *Ren7* loci and their PM-susceptible alternative haplotypes using progeny genomes. Alignment of the genome assemblies of six 11373 sib-lines onto *Ren6*, *Ren7*, and their PM-susceptible (PMS) alternatives from *V. piazeskii* DVIT2027 (**a**) and *V. vinifera* F2-35 (**b**). Each square represents a contig sequence.

Gene annotation, combined with the identification of potential NLR gene loci and manual refinement of gene models, revealed differences in the number of genes, particularly NLR genes, between the PMR loci and their PMS counterparts (**Table 2**). Nineteen and thirteen NLR genes were annotated within the *Ren6* and *Ren7*, respectively. In *Ren6*, two NLR genes were located between markers PN9-063 and PN9-066.1 (202.6 kbp), while the remaining NLR genes clustered between PN9-067 and VMC4h4.1 (664.3 kbp) (**Figure 2a**). In Pap *et al*. (Pap et al., 2016), *Ren6* was positioned between PN9-063 and PN9-067.2 based on QTL analysis. However, markers PN9-067.2 and PN9-068 amplified in multiple locations, complicating precise mapping and reducing the ability to narrow down candidate NLR (**Table S11**). Notably, the *Ren6*-PMS alternative haplotype of *V. piazeskii* DVIT2027 (35) contained more NLR genes than the PMR haplotype (20). The region carrying the NLR genes of the *Ren6* locus spanned 747.9 kbp whereas the PMS alternative region was 1,209.3 kbp, explaining the length difference between the two haplotypes. In contrast, *Ren7* was composed of a greater number of NLR genes (13) compared to its PMS counterpart (8). The NLR genes of *Ren7* and its PMS alternative haplotype clustered within a 266.2 and 183.9 kbp region, respectively, between markers VMC9a2.1 and VMC5h11 (606.5 and 621.4 kbp, respectively) (**Figure 2b**), matching previously defined locus boundaries (Pap et al., 2016).

In both *Ren6* and *Ren7*, most NLR genes encoded CC-NBS-LRR proteins (**Table 2**; **Table S12**). In *V. vinifera* F2-35, twelve NLR genes were annotated in each *Ren6*-PMS haplotype, while only two and three NLR genes were identified in the *Ren7*-PMS haplotypes.

Comparison of *Ren6* and *Ren7* loci with their PM-susceptible alternative haplotypes

To identify NLR(s) potentially associated with *Ren6* and *Ren7* genetic PM resistance, we compared the PMR loci with their respective PMS alternative haplotypes. For *Ren6*, few short structural variations (SVs; > 50bp) were detected between markers PN9-063 and PN9-066.1 (202.6 in *Ren6 vs.* 183 kbp in its PMS counterpart) (**Figure 2a**). In contrast, numerous large SVs, particularly duplications, were identified between PN9-067 and VMC4h4.1 (664.3 in *Ren6 vs.* 1,078.9 kbp in its PMS counterpart), largely explaining the length difference between the two haplotypes. These SVs disrupted the coding sequences (CDS) of ten NLR genes and altered their domain composition (**Figure 2a**; **Table S13**).

For *Ren7*, a large complex SV spanned from 955.0 to 1,088.6 kbp (133.6 kbp) on Haplotype 1 of chromosome 19 of *V. piazeskii* DVIT2027 relative to Haplotype 2 (**Figure 2b**). This SV affected the CDS of five NLR genes (**Table S14**), explaining the difference of NLR gene number between the two haplotypes. Two additional NLR genes (g332390 and g332430), both located downstream in the *Ren7* locus, were impacted by duplication events (**Figure 2b**; **Table S14**). Comparable SVs were also observed when comparing the PMS haplotypes of *V. vinifera* F2-35 with the *Ren6* and *Ren7* loci (**Figure S9**).

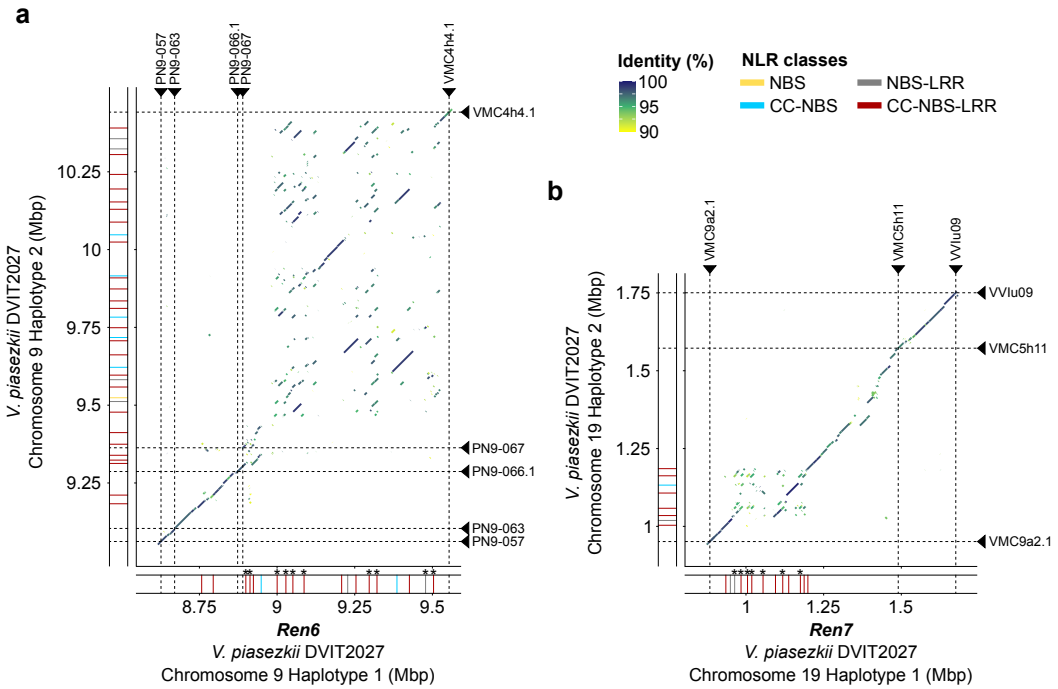

Figure 2: Effect of the structural variations between *Ren6* and *Ren7* loci and their PM-susceptible alternative haplotypes on the NLR gene content. Alignment of the PM-susceptible alternative haplotypes of *Ren6* (**a**) and *Ren7* (**b**) from *V. piasezkii* DVIT2027 onto their PM-resistant counterparts. Chromosomal positions of the NLR genes composing the four haplotypes are represented by colored rectangles, which color indicates the NLR class. NLR genes in *Ren6* and *Ren7* which protein-coding sequence is impacted by a structural variation are indicated by an asterisk.

375 In addition to SVs, we identified small polymorphisms, including 46,178 and 20,669 SNPs and
376 6,629 and 3,928 INDELs (< 50 bp) in *Ren6* and *Ren7*, respectively (**Tables S15-S16**). Comparison
377 with the CDS of the NLR genes showed that all the NLRs in *Ren6* and *Ren7* were affected by
378 small polymorphisms, suggesting that the two loci are highly polymorphic.
379
380 To further assess the impact of SVs and small polymorphisms on NLR gene content, we analyzed
381 allele relationships by constructing phylogenetic trees for the NLR genes at each *R* locus (**Figure**
382 **3**). In *V. piazeskii* DVIT2027, 2 of the 19 NLR (10.5%) genes in *Ren6* (g158080.m01, and
383 g158100.m01) and 6 out of 13 NLR genes (46.1%) in *Ren7* (g332310, g332320, g332340,
384 g332350, g332390, g332430) did not possess an allelic counterpart in their respective PMS
385 haplotypes (**Tables S13-S14**). Although some of those genes have an allelic counterpart in *V.*
386 *vinifera* F2-35, the absence of an allelic form in the PMS haplotypes from *V. piasezkii* DVIT2027
387 suggests that they could be potentially involved in *Ren6*- and *Ren7*-mediated PM resistance.
388 Noteworthily, none of the allele pairs showed identical protein sequences, suggesting that all NLRs
389 in *Ren6* and *Ren7* are specific to the PMR haplotypes and differ from their PMS counterparts.
390
391 Altogether these results show that SVs and small polymorphisms impact on both number and
392 sequence of the NLR genes in *Ren6* and *Ren7* relatively to their PMS counterparts, making all the
393 NLRs composing *Ren6* and *Ren7* potentially responsible for PM resistance.

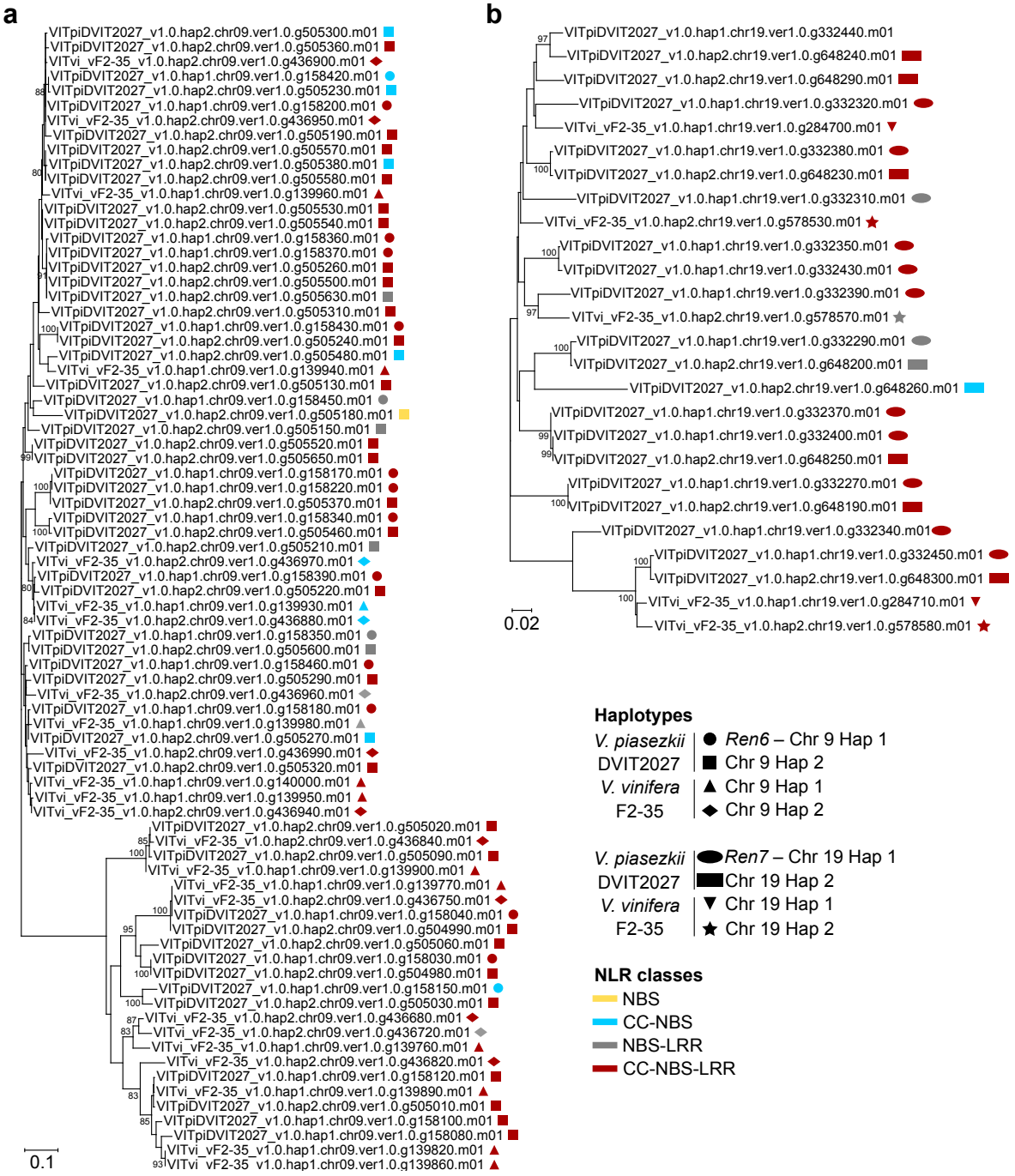

Figure 3: Identification of allele relationship between NLRs composing *Ren6* and *Ren7*, and their PM-susceptible alternative haplotypes, based on phylogeny. Neighbor-joining clustering of the predicted NLR sequences composing *Ren6* (**a**) and *Ren7* (**b**), and their PM-susceptible alternative haplotypes. Scale bar is in the unit of the number of substitutions per site. Bootstrap values greater than 80 are indicated.

Identification of expressed NLR genes within *Ren6* and *Ren7*

To narrow down the NLR genes potentially responsible for *Ren6*- and *Ren7*-mediated PM resistance, we analyzed their expression in leaves of six 11373 sib-lines carrying *Ren6*, *Ren7*, or both *R* loci. Leaves were collected one and five days after inoculation with *E. necator* or a mock

solution. Within *Ren6*, four CC-NBS-LRR genes were consistently expressed (>0.2 TPM) in all the *Ren6*$^{+}$ accessions, both constitutively and in response to *E. necator*. One gene (g158030) was located between markers PN9-063 and PN9-066.1, while the other three (g158080; g158100; g158430) were located between PN9-067 and VMC4h4.1 (**Figure 4a**). Interestingly, two of these genes (g158080 and g158100) lack allelic counterparts in the PMS haplotype of *V. piazeskii* DVIT2027. For *Ren7*, two CC-NBS-LRR genes were expressed within the interval between markers VMC9a2.1 and VMC5h11 (g332380 and g332390), including one without an allelic counterpart in the PMS haplotype (g332390).

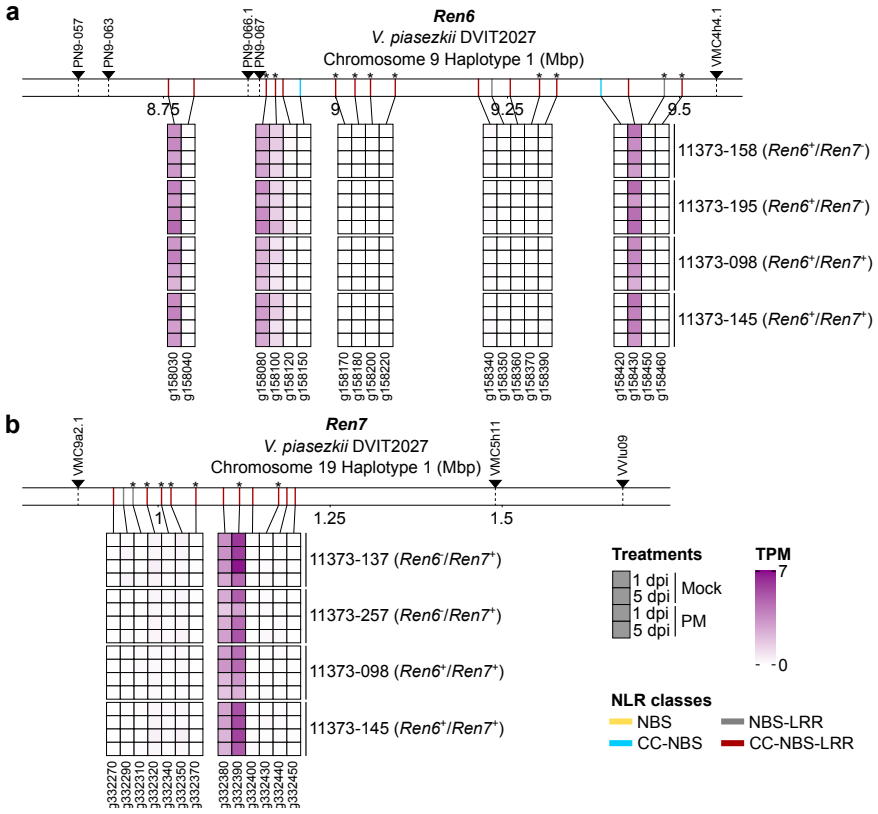

Figure 4: Identification of candidate NLRs responsible for PM resistance within *Ren6* and *Ren7* based on constitutive gene expression. Transcript abundance of the NLR genes belonging to *Ren6* (**a**) and *Ren7* (**b**) loci. Gene expression was measured in 11373 sib-lines possessing either *Ren6, Ren7*, or both *R* loci, at one and five days post-inoculation (dpi) with a mock solution (Mock) or *E. necator* conidia (PM). For each condition, transcript abundance is represented as the mean of transcript per million (TPM) of three bioreplicates (n = 3). Chromosomal positions of the NLR genes composing the four haplotypes are represented by colored rectangles, with the color indicating the NLR class. NLR genes which protein-coding sequence is impacted by at least one structural variation relative to the alternative PMS haplotype of *V. piazeskii* DVIT2027 are indicated by an asterisk.

Altogether, our results point to four (g158030; g158080; g158100; g158430) and two (g332380 and g332390) candidate CC-NBS-LRR genes associated with *Ren6* and *Ren7* resistance, respectively, based on their consistent expression in PMR sib-lines, and their absence or sequence divergence in the corresponding PMS haplotype (**Figure 5**). The candidates g158080 and g158100 from *Ren6*, and g332390 from *Ren7*, do not possess an allelic form in their respective PMS haplotype in *V. piazeskii* DVIT2027. The proteins encoded by g158030 and g158430 from *Ren6* have 2 and 1 amino acid changes compared to their allelic counterparts in the PMS haplotype of

V. piazeskii DVIT2027 (**Figure 5a**), including an amino acid change located in the CC domain of first one. Relatively to its PMS allele, the predicted protein of g332380 from *Ren7* has 2 amino acid changes, including one in the NB-ARC domain, as well as 2 deletions of 5 and 91 amino acids at the end of the protein (**Figure 5b**).

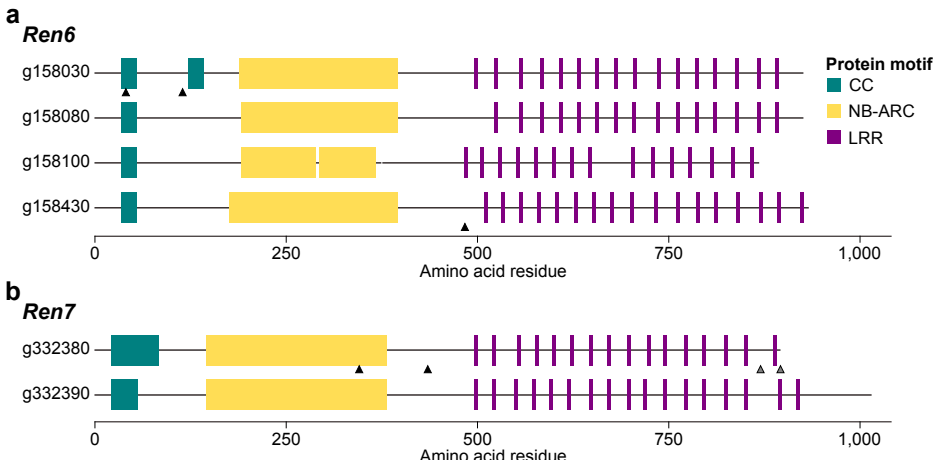

Figure 5: Candidate CC-NBS-LRRs associated with the PM resistance of *Ren6* and *Ren7* of *V. piasezkii* DVIT2027. Protein motif composition of the candidate CC-NBS-LRRs among *Ren6* (**a**) and *Ren7* (**b**) loci. Black and gray triangles indicate the position of the amino changes and deletions compared to the allelic counterpart located in the PM-susceptible haplotype of *V. piasezkii* DVIT2027, respectively.

Discussion

By integrating the haplotype-resolved, T2T genomes of the two parents, PM-resistant *V. piasezkii* DVIT2027 and PM-susceptible *V. vinifera* F2-35, with the phased genomes of six of their progeny, we were able to precisely locate and validate the phasing, structure, and sequence of the *Ren6* and *Ren7* loci in *V. piasezkii DVIT2027*. While both R loci and their PMS haplotypes in *V. vinifera* F2-35 were resolved within single contigs in at least one sib-line, the PMS alternative haplotypes in *V. piasezkii* DVIT2027 remained fragmented in all sib-lines (**Figure 1**). This highlights the challenges of assembling highly repetitive and structurally complex regions, particularly when using CLR data.

Alignments of the PMS alternative haplotypes onto *Ren6* and *Ren7* showed large and complex SVs in the regions containing the NLR genes, as well as several short polymorphisms (**Figure 2**). Similar results were found when comparing the two haplotypes of *Run1.2* and *Run2.2* of *M. rotundifolia* Trayshed (Massonnet et al., 2022b). This suggests that, like in many angiosperms, NLR clusters in grapes have undergone a diversification at both inter- and intra-species levels, likely in response to strong selection pressures from pathogens (Contreras et al., 2023). Phylogenetic trees of the NLRs of both PMR and PMS haplotypes (**Figure 3**) showed that the SVs and small polymorphisms between haplotypes led to allele presence/absence, pointing out NLRs from *Ren6* and *Ren7* without allelic counterparts in their respective PMS haplotype. Furthermore, sequence comparison showed that all the NLR protein sequences from *Ren6* and *Ren7* were specific to the two PMR haplotypes. Additional sequence comparisons determined that only two NLR genes within *Ren6* (g158370 and g158460) had an identical protein sequence in the *V. piazeskii* accessions 0957 and BL-1 (Guo et al., 2025b), emphasizing the specificity of the NLR content of *Ren6* and *Ren7* in the accession DVIT2027. Further investigation of other PMR *V.*

467 *piasezkii* accessions, such as DVIT2032 (Riaz et al., 2013), could reveal whether they carry PMR
468 haplotypes at *Ren6* and *Ren7* and help identify additional resistance genes or alleles.
469
470 In addition to use genomes of 11373 sib-lines in our pipeline of identification of candidate NLR
471 genes, we integrated transcriptomic data from leaves of six 11373 sib-lines carrying *Ren6*, *Ren7*,
472 or both *R* loci, in presence or absence of the pathogen. Based on their constitutive expression
473 (**Figure 4**), and their absence or sequence divergence in their respective PMS haplotype from *V.*
474 *piasezkii* DVIT2027 (**Figure 5**), we identified four (g158030; g158080; g158100; g158430) and
475 two (g332380 and g332390) candidate CC-NBS-LRR genes associated with *Ren6* and *Ren7*
476 resistance, respectively. Genomic and/or transcriptomic data from additional recombinants would
477 help to narrow down candidate NLRs, especially in *Ren6*, considering that g158100 and g158430
478 are 508.7 kbp apart.
479
480 The extensive structural variation and gene presence/absence observed at *Ren6* and *Ren7* suggest
481 localized expansion and deletion events, likely driven by transposable element (TE) activity,
482 unequal crossing-over, and other recombination-based mechanisms. These processes are well-
483 established contributors to the diversification of NBS-LRR gene clusters, promoting rapid
484 sequence evolution, gene copy number variation, and the emergence of novel specificities (Jacob
485 et al., 2013; Contreras et al., 2023). Similar levels of structural and sequence variability have been
486 reported at other grape *R* loci, including *Run1* (Feechan et al., 2013), *Run1.2* and *Run2.2* in *M.*
487 *rotundifolia* (Cochetel et al., 2021; Massonnet et al., 2022b), *Resistance to Plasmopara viticola* 3
488 (*Rpv*3) in eight *Vitis* accessions (Wilkerson et al., 2025), and *Rpv33* in *Vitis* × *doaniana* (Zou et
489 al., 2023), suggesting that such dynamic architecture is a common feature of resistance loci in
490 *Vitis*. With the growing availability of high-quality, phased genomes from diverse *Vitis* species
491 (Cantu et al., 2024), we are now well positioned to explore the evolutionary trajectories of *R* loci
492 across the genus. Systematic comparisons will allow us to investigate patterns of NLR gene birth
493 and loss, the influence of TEs and local recombination rates, and the selective pressures shaping
494 resistance gene repertoires in *Vitis* (Jacob et al., 2013; Contreras et al., 2023; Guo et al., 2025a).
495
496 From a breeding perspective, the sequence-level resolution of these loci and their candidate genes
497 opens new paths for precise marker development. Given the complete haplotype specificity of
498 these NLRs, these markers could enable rapid screening in breeding programs or precise gene
499 editing (Greenwood et al., 2023). Stacking *Ren6* and *Ren7* with other resistance loci like *Run1* and
500 *Ren4* is in progress in multiple breeding programs to reduce the risk of resistance breakdown.
501
502 Technically, our results highlight the power of phased diploid assemblies and integrated pipelines
503 that combine long-read sequencing, high-quality phasing, and expression profiling. However, they
504 also underscore the continued need for manual validation and careful curation of locus structure
505 and gene models (Cantu et al., 2024). The fragmentation of some haplotypes assembled with
506 PacBio CLR data further supports the shift toward HiFi technology, or other high-fidelity
507 technologies for resolving complex *R* loci.
508
509 Future work will focus on functional validation of the six candidate genes, potentially through
510 gene knockouts using genome editing, complementation in susceptible backgrounds via stable
511 transformation, and targeted knock-ins once such methods become available in grapevine
512 (Greenwood et al., 2023; Schreiber et al., 2024). Their response to a broader panel of *E. necator*

isolates will also be assessed. Identifying the gene(s) truly responsible for PM resistance will enable the development of perfect markers to support marker-assisted selection, reducing linkage drag from wild *Vitis* species. In parallel, defining precise *R* gene targets will provide a valuable foundation for future gene editing strategies aimed at accelerating resistance breeding while preserving varietal identity (Ren et al., 2024).

Acknowledgments

This work was funded by the USDA NIFA Award #2022-51181-38240.

Author contributions

M.M., and D.C. designed the project; M.A.W. provided plant material; M.M., S.M., and D.P. collected the plant material; R.F.-B. extracted DNA and RNA, and prepared sequencing libraries; M.M. and N.C. performed the data analyses; M.M. and D.C. wrote the manuscript.

Data availability

Sequencing data and are accessible through NCBI under the BioProject PRJNA1258375. Genome sequences and their annotation files are available at Zenodo doi:10.5281/zenodo.15361017.

Conflict of interest

The authors declare that they have no conflicts of interest.

References

Altschul SF, Gish W, Miller W, Myers EW, Lipman DJ (1990) Basic local alignment search tool. J Mol Biol **215**: 403–410

Amrine KCH, Blanco-Ulate B, Riaz S, Pap D, Jones L, Figueroa-Balderas R, Walker MA, Cantu D (2015) Comparative transcriptomics of Central Asian Vitis vinifera accessions reveals distinct defense strategies against powdery mildew. Hortic Res **2**: 15037

Barnett DW, Garrison EK, Quinlan AR, Strömberg MP, Marth GT (2011) BamTools: a C++ API and toolkit for analyzing and managing BAM files. Bioinformatics **27**: 1691–1692

Bolger AM, Lohse M, Usadel B (2014) Trimmomatic: a flexible trimmer for Illumina sequence data. Bioinformatics **30**: 2114–2120

Calonnec A, Cartolaro P, Poupot C, Dubourdieu D, Darriet P (2004) Effects of Uncinula necator on the yield and quality of grapes (Vitis vinifera) and wine. Plant Pathol **53**: 434–445

Cantu D, Massonnet M, Cochetel N (2024) The wild side of grape genomics. Trends Genet **40**: 601–612

Cheng H, Concepcion GT, Feng X, Zhang H, Li H (2021) Haplotype-resolved de novo assembly using phased assembly graphs with hifiasm. Nat Methods **18**: 170–175

Chia K-S, Carella P (2023) Taking the lead: NLR immune receptor N-terminal domains execute plant immune responses. New Phytol **240**: 496–501

Chin C-S, Peluso P, Sedlazeck FJ, Nattestad M, Concepcion GT, Clum A, Dunn C, O'Malley R, Figueroa-Balderas R, Morales-Cruz A, et al (2016) Phased Diploid Genome Assembly with Single Molecule Real-Time Sequencing. Nat Methods **13**: 1050–1054

Cochetel N, Minio A, Guarracino A, Garcia JF, Figueroa-Balderas R, Massonnet M, Kasuga T, Londo JP, Garrison E, Gaut BS, et al (2023) A super-pangenome of the North American wild grape species. Genome Biol **24**: 290

Cochetel N, Minio A, Massonnet M, Vondras AM, Figueroa-Balderas R, Cantu D (2021) Diploid chromosome-scale assembly of the Muscadinia rotundifolia genome supports chromosome fusion and disease resistance gene expansion during Vitis and Muscadinia divergence. G3 GenesGenomesGenetics **11**: jkab033

Contreras MP, Lüdke D, Pai H, Toghani A, Kamoun S (2023) NLR receptors in plant immunity: making sense of the alphabet soup. EMBO Rep **24**: e57495

Dry I, Riaz S, Fuchs M, Sosnowski M, Thomas M (2019) Scion Breeding for Resistance to Biotic Stresses. *In* D Cantu, MA Walker, eds, Grape Genome. Springer International Publishing, Cham, pp 319–347

El-Gebali S, Mistry J, Bateman A, Eddy SR, Luciani A, Potter SC, Qureshi M, Richardson LJ, Salazar GA, Smart A, et al (2019) The Pfam protein families database in 2019. Nucleic Acids Res **47**: D427–D432

Feechan A, Anderson C, Torregrosa L, Jermakow A, Mestre P, Wiedemann-Merdinoglu S, Merdinoglu D, Walker AR, Cadle-Davidson L, Reisch B, et al (2013) Genetic dissection of a TIR-NB-LRR locus from the wild North American grapevine species Muscadinia rotundifolia identifies paralogous genes conferring resistance to major fungal and oomycete pathogens in cultivated grapevine. Plant J Cell Mol Biol **76**: 661–674

Foria S, Magris G, Jurman I, Schwope R, De Candido M, De Luca E, Ivanišević D, Morgante M, Di Gaspero G (2022) Extent of wild–to–crop interspecific introgression in grapevine (*Vitis vinifera*) as a consequence of resistance breeding and implications for the crop species definition. Hortic Res **9**: uhab010

Gadoury DM, Cable-Davidson L, Wilcox WF, Dry IB, Seem RC, Milgroom MG (2011) Grapevine powdery mildew (Erysiphe necator): a fascinating system for the study of the biology, ecology and epidemiology of an obligate biotroph. Mol Plant Pathol **13**: 1–16

Greenwood JR, Zhang X, Rathjen JP (2023) Precision genome editing of crops for improved disease resistance. Curr Biol **33**: R650–R657

Guo B-C, Zhang Y-R, Liu Z-G, Li X-C, Yu Z, Ping B-Y, Sun Y-Q, van den Burg H, Ma F-W, Zhao T (2025a) Deciphering Plant NLR Genomic Evolution: Synteny-Informed Classification Unveils Insights into TNL Gene Loss. Mol Biol Evol **42**: msaf015

Guo L, Wang X, Ayhan DH, Rhaman MS, Yan M, Jiang J, Wang D, Zheng W, Mei J, Ji W, et al (2025b) Super pangenome of Vitis empowers identification of downy mildew resistance genes for grapevine improvement. Nat Genet **57**: 741–753

Haas BJ, Salzberg SL, Zhu W, Pertea M, Allen JE, Orvis J, White O, Buell CR, Wortman JR (2008) Automated eukaryotic gene structure annotation using EVidenceModeler and the Program to Assemble Spliced Alignments. Genome Biol **9**: R7

Jacob F, Vernaldi S, Maekawa T (2013) Evolution and Conservation of Plant NLR Functions. Front Immunol. doi: 10.3389/fimmu.2013.00297

Jaillon O, Aury JM, Noel B, Policriti A, Clepet C, Casagrande A, Choisne N, Aubourg S, Vitulo N, Jubin C, et al (2007) The grapevine genome sequence suggests ancestral hexaploidization in major angiosperm phyla. Nature **449**: 463–468

Jones L, Riaz S, Morales-Cruz A, Amrine KC, McGuire B, Gubler WD, Walker MA, Cantu D (2014) Adaptive genomic structural variation in the grape powdery mildew pathogen, Erysiphe necator. BMC Genomics **15**: 1081

Karn A, Zou C, Brooks S, Fresnedo-Ramírez J, Gabler F, Sun Q, Ramming D, Naegele R, Ledbetter C, Cadle-Davidson L (2021) Discovery of the REN11 Locus From Vitis aestivalis for Stable Resistance to Grapevine Powdery Mildew in a Family Segregating for Several Unstable and Tissue-Specific Quantitative Resistance Loci. Front Plant Sci. doi: 10.3389/fpls.2021.733899

Kim D, Langmead B, Salzberg SL (2015) HISAT: a fast spliced aligner with low memory requirements. Nat Methods **12**: 357–360

Koren S, Rhie A, Walenz BP, Dilthey AT, Bickhart DM, Kingan SB, Hiendleder S, Williams JL, Smith TPL, Phillippy AM (2018) De novo assembly of haplotype-resolved genomes with trio binning. Nat Biotechnol 10.1038/nbt.4277

Li H, Durbin R (2009) Fast and accurate short read alignment with Burrows–Wheeler transform. Bioinformatics **25**: 1754–1760

Locci F, Parker JE Plant NLR immunity activation and execution: a biochemical perspective. Open Biol **14**: 230387

Lolle S, Stevens D, Coaker G (2020) Plant NLR triggered immunity: From receptor activation to downstream signaling. Curr Opin Immunol **62**: 99–105

Lomsadze A, Ter-Hovhannisyan V, Chernoff YO, Borodovsky M (2005) Gene identification in novel eukaryotic genomes by self-training algorithm. Nucleic Acids Res **33**: 6494–6506

Lupas A, Van Dyke M, Stock J (1991) Predicting coiled coils from protein sequences. Science **252**: 1162–1164

Marçais G, Delcher AL, Phillippy AM, Coston R, Salzberg SL, Zimin A (2018) MUMmer4: A fast and versatile genome alignment system. PLoS Comput Biol **14**: e1005944

Martin EC, Sukarta OCA, Spiridon L, Grigore LG, Constantinescu V, Tacutu R, Goverse A, Petrescu A-J (2020) LRRpredictor—A New LRR Motif Detection Method for Irregular Motifs of Plant NLR Proteins Using an Ensemble of Classifiers. Genes **11**: 286

Massonnet M, Cochetel N, Minio A, Vondras AM, Lin J, Muyle A, Garcia JF, Zhou Y, Delledonne M, Riaz S, et al (2020) The genetic basis of sex determination in grapes. Nat Commun **11**: 2902

Massonnet M, Riaz S, Pap D, Figueroa-Balderas R, Walker MA, Cantu D (2022a) The grape powdery mildew resistance loci Ren2, Ren3, Ren4D, Ren4U, Run1, Run1.2b, Run2.1, and Run2.2 activate different transcriptional responses to Erysiphe necator. Front Plant Sci **13**: 1096862

Massonnet M, Vondras AM, Cochetel N, Riaz S, Pap D, Minio A, Figueroa-Balderas R, Walker MA, Cantu D (2022b) Haplotype-resolved powdery mildew resistance loci reveal the impact of heterozygous structural variation on NLR genes in Muscadinia rotundifolia. G3 GenesGenomesGenetics **12**: jkac148

Minio A, Cochetel N, Massonnet M, Figueroa-Balderas R, Cantu D (2022a) HiFi chromosome-scale diploid assemblies of the grape rootstocks 110R, Kober 5BB, and 101–14 Mgt. Sci Data **9**: 660

Minio A, Cochetel N, Vondras AM, Massonnet M, Cantu D (2022b) Assembly of complete diploid-phased chromosomes from draft genome sequences. G3 GenesGenomesGenetics **12**: jkac143

Minio A, Massonnet M, Figueroa-Balderas R, Castro A, Cantu D (2019a) Diploid Genome Assembly of the Wine Grape Carménère. G3 GenesGenomesGenetics **9**: 1331–1337

Minio A, Massonnet M, Figueroa-Balderas R, Vondras AM, Blanco-Ulate B, Cantu D (2019b) Iso-Seq Allows Genome-Independent Transcriptome Profiling of Grape Berry Development. G3 GenesGenomesGenetics **9**: 755–767

Paineau M, Zaccheo M, Massonnet M, Cantu D (2024) Advances in grape and pathogen genomics toward durable grapevine disease resistance. J Exp Bot erae450

Pap D, Riaz S, Dry IB, Jermakow A, Tenscher AC, Cantu D, Oláh R, Walker MA (2016) Identification of two novel powdery mildew resistance loci, Ren6 and Ren7, from the wild Chinese grape species Vitis piasezkii. BMC Plant Biol **16**: 170

Quinlan AR (2014) BEDTools: the Swiss-army tool for genome feature analysis. Curr Protoc Bioinforma Ed Board Andreas Baxevanis Al **47**: 11.12.1-11.12.34

Ren C, Mohamed MSM, Aini N, Kuang Y, Liang Z (2024) CRISPR/Cas in Grapevine Genome Editing: The Best Is Yet to Come. Horticulturae **10**: 965

Riaz S, Boursiquot J-M, Dangl GS, Lacombe T, Laucou V, Tenscher AC, Walker MA (2013) Identification of mildew resistance in wild and cultivated Central Asian grape germplasm. BMC Plant Biol **13**: 149

Ricciardi V, Crespan M, Maddalena G, Migliaro D, Brancadoro L, Maghradze D, Failla O, Toffolatti SL, De Lorenzis G (2024) Novel loci associated with resistance to downy and powdery mildew in grapevine. Front Plant Sci. doi: 10.3389/fpls.2024.1386225

Robinson JT, Thorvaldsdóttir H, Winckler W, Guttman M, Lander ES, Getz G, Mesirov JP (2011) Integrative Genomics Viewer. Nat Biotechnol **29**: 24–26

Sambucci O, Alston JM, Fuller KB, Lusk J (2019) The Pecuniary and Nonpecuniary Costs of Powdery Mildew and the Potential Value of Resistant Grape Varieties in California. Am J Enol Vitic **70**: 177–187

Schreiber T, Prange A, Schäfer P, Iwen T, Grützner R, Marillonnet S, Lepage A, Javelle M, Paul W, Tissier A (2024) Efficient scar-free knock-ins of several kilobases in plants by engineered CRISPR-Cas endonucleases. Mol Plant **17**: 824–837

Stanke M, Keller O, Gunduz I, Hayes A, Waack S, Morgenstern B (2006) AUGUSTUS: ab initio prediction of alternative transcripts. Nucleic Acids Res **34**: W435–W439

Steuernagel B, Witek K, Krattinger SG, Ramirez-Gonzalez RH, Schoonbeek H, Yu G, Baggs E, Witek AI, Yadav I, Krasileva KV, et al (2020) The NLR-Annotator Tool Enables Annotation of the Intracellular Immune Receptor Repertoire1[OPEN]. Plant Physiol **183**: 468–482

Stummer BE, Francis IL, Zanker T, Lattey KA, Scott ES (2005) Effects of powdery mildew on the sensory properties and composition of Chardonnay juice and wine when grape sugar ripeness is standardised. Aust J Grape Wine Res **11**: 66–76

Trapnell C, Williams BA, Pertea G, Mortazavi A, Kwan G, van Baren MJ, Salzberg SL, Wold BJ, Pachter L (2010) Transcript assembly and abundance estimation from RNA-Seq reveals thousands of new transcripts and switching among isoforms. Nat Biotechnol **28**: 511–515

Wang M, Kong L (2019) pblat: a multithread blat algorithm speeding up aligning sequences to genomes. BMC Bioinformatics **20**: 28

Waterhouse RM, Seppey M, Simão FA, Manni M, Ioannidis P, Klioutchnikov G, Kriventseva EV, Zdobnov EM (2018) BUSCO Applications from Quality Assessments to Gene Prediction and Phylogenomics. Mol Biol Evol **35**: 543–548

Wilkerson D, Zou C, Sun Q, Nigar Q, Paineau M, Cantu D, Hwang C-F, Cadle-Davidson L (2025) Comparative genomics of *Rpv3*, a multiallelic downy mildew resistance locus in grapevine (*Vitis* sp.). OENO One. doi: 10.20870/oeno-one.2025.59.1.8244

Wu TD, Watanabe CK (2005) GMAP: a genomic mapping and alignment program for mRNA and EST sequences. Bioinforma Oxf Engl **21**: 1859–1875

Zou C, Sapkota S, Figueroa-Balderas R, Glaubitz J, Cantu D, Kingham BF, Sun Q, Cadle-Davidson L (2023) A multitiered haplotype strategy to enhance phased assembly and fine mapping of a disease resistance locus. Plant Physiol **193**: 2321–2336

1